

Electronic properties of GeTe and Ag- or Sb-substituted GeTe studied by low-temperature ^{125}Te NMR

J. Cui,^{1,2} E. M. Levin,^{1,3} Y. Lee,¹ and Y. Furukawa^{1,3}

¹*Ames Laboratory, U.S. DOE, Iowa State University, Ames, Iowa 50011, USA*

²*Department of Chemistry, Iowa State University, Ames, Iowa 50011, USA*

³*Department of Physics and Astronomy, Iowa State University, Ames, Iowa 50011, USA*

(Received 21 June 2016; revised manuscript received 28 July 2016; published 18 August 2016)

We have carried out ^{125}Te nuclear magnetic resonance (NMR) in a wide temperature range of 1.5–300 K to investigate the electronic properties of $\text{Ge}_{50}\text{Te}_{50}$, $\text{Ag}_2\text{Ge}_{48}\text{Te}_{50}$, and $\text{Sb}_2\text{Ge}_{48}\text{Te}_{50}$ from a microscopic point of view. From the temperature dependence of the NMR shift (K) and nuclear spin lattice relaxation rate ($1/T_1$), we found that two bands contribute to the physical properties of the materials. One band overlaps the Fermi level providing the metallic state where no strong electron correlations are revealed by Korringa analysis. The other band is separated from the Fermi level by an energy gap of $E_g/k_B \sim 67$ K, which gives rise to semiconductorlike properties. First-principles calculation reveals that the metallic band originates from the Ge vacancy while the semiconductorlike band is related to the fine structure of the density of states near the Fermi level. Low-temperature ^{125}Te NMR data for the materials studied here clearly show that Ag substitution increases hole concentration while Sb substitution decreases it.

DOI: [10.1103/PhysRevB.94.085203](https://doi.org/10.1103/PhysRevB.94.085203)

I. INTRODUCTION

Complex tellurides have been studied extensively due to their intriguing fundamental properties and their application as thermoelectric materials [1–6], which directly convert heat into electricity. The efficiency is characterized by the dimensionless figure of merit $zT = S^2\sigma T/\kappa$ (S the Seebeck coefficient, σ the electrical conductivity, T the absolute temperature, and κ the thermal conductivity). The well-known group of thermoelectric materials, the complex tellurides based on GeTe [7–9], TAGS- m materials $(\text{GeTe})_m(\text{AgSbTe}_2)_{100-m}$, have a thermoelectric figure of merit zT above 1 [6,10–12]. According to band calculations, GeTe is a narrow-band-gap semiconductor whose band gap is calculated to be 0.3–0.5 eV [13–16]. On the other hand, electrical resistivity measurements show metallic behavior [7,17–20], although a small gap also has been observed by optical measurements [21]. This is believed to be due to high hole concentrations generated by Ge vacancies, forming a self-dopant system with p -type conductivity [7,17,22]. Therefore, depending on the samples' composition, they may have different concentrations of Ge vacancies, resulting in different physical properties. This makes it very difficult to understand the physical properties of GeTe-based materials. In fact, there is a significant discrepancy between the electronic and thermal transport data for GeTe-based materials reported in the literature [6,23–25].

To avoid such confusion, one needs to study the physical properties using well-characterized samples. We have conducted a systematic characterization of GeTe by using x-ray diffraction (XRD), scanning electron microscopy (SEM), energy dispersive spectroscopy (EDS), Seebeck coefficient, electrical resistivity, Hall effect, thermal conductivity, and ^{125}Te nuclear magnetic resonance (NMR) measurements [7]. Hereafter, we will use the notation $\text{Ge}_{50}\text{Te}_{50}$ for GeTe with the coefficients shown in atomic percent.

In our previous paper [7], we concluded that the discrepancy in the data for $\text{Ge}_{50}\text{Te}_{50}$ reported in the literature can be attributed to the variation in the Ge/Te ratio of solidified

samples as well as to different conditions of measurements. It is well established that NMR is a powerful tool to investigate carrier concentrations in semiconductors from a microscopic point of view. The Hall and Seebeck effects show only bulk properties, which can be affected by small amounts of a second phase [26,27]. Nuclear spin lattice relaxation rates ($1/T_1$) have been measured at room temperature, and were found to increase linearly with carrier concentrations [28]. However, to our knowledge, no systematic NMR investigation of $\text{Ge}_{50}\text{Te}_{50}$ has been carried out over a wide temperature range.

In this paper, we report ^{125}Te NMR measurements of $\text{Ge}_{50}\text{Te}_{50}$ over a wide temperature range of $T = 1.5\text{--}300$ K. We found that the NMR shift K and $1/T_1T$ data are nearly temperature independent at temperatures below ~ 50 K and both increase slightly with increasing temperature at high temperatures. These behaviors can be explained well by a two-band model, where one band overlaps the Fermi level and the other band is separated from the Fermi level by an energy gap of $E_g/k_B \sim 67$ K. First-principles calculations indicate that the first band originates from the Ge vacancy while the second band is related to the fine structure of the density of states near the Fermi level. We also carried out ^{125}Te NMR measurements of $M_2\text{Ge}_{48}\text{Te}_{50}$ ($M = \text{Ag, Sb}$) to study the carrier doping effects on the electronic properties. Clear changes in carrier concentration upon Ag or Sb substitutions were observed: Ag substitution increases the hole concentration whereas Sb substitution decreases the concentration, which is consistent with our previous report [29].

II. EXPERIMENT

Polycrystalline samples of $\text{Ge}_{50}\text{Te}_{50}$, $\text{Ag}_2\text{Ge}_{48}\text{Te}_{50}$, and $\text{Sb}_2\text{Ge}_{48}\text{Te}_{50}$ were prepared by a direct reaction of the constituent elements of Ge, Te, Ag, or Sb in fused silica ampoules, as described in Refs. [7,29]. The samples were well characterized by XRD, Seebeck coefficient, electrical resistivity, Hall effects, and room-temperature ^{125}Te NMR

measurements. The coarsely powdered samples were loosely packed into 6-mm quartz tubes for NMR measurements. NMR measurements of ^{125}Te ($I = \frac{1}{2}$, $\frac{\gamma_N}{2\pi} = 13.464 \text{ MHz/T}$) were conducted using a homemade phase-coherent spin-echo pulse spectrometer. ^{125}Te NMR spectra were obtained either by a Fourier transform of the NMR echo signal at a constant magnetic field of 7.4089 T or by sweeping the magnetic field at a frequency of 99.6 MHz in the temperature range of $T = 1.5\text{--}300 \text{ K}$. The NMR echo signal was obtained by means of a Hahn echo sequence with a typical $\pi/2$ radio-frequency (rf) pulse length of $7.5 \mu\text{s}$ which produces an oscillation field (so-called H_1) of $\sim 25 \text{ Oe}$.

III. RESULTS AND DISCUSSION

Figure 1 shows field-swept ^{125}Te NMR spectra measured at 4.3 K for $\text{Ge}_{50}\text{Te}_{50}$, $\text{Ag}_2\text{Ge}_{48}\text{Te}_{50}$, and $\text{Sb}_2\text{Ge}_{48}\text{Te}_{50}$. The full width at half maximum (FWHM) for $\text{Ge}_{50}\text{Te}_{50}$ is 40.0(5) Oe at $T = 4.3 \text{ K}$, which is almost independent of temperature, although a slight increase can be observed below $\sim 25 \text{ K}$, as shown in the inset of Fig. 1. This FWHM is slightly smaller than 43 Oe at room temperature, as reported previously [29]. With Ag substitution the peak position shifts to a lower magnetic field, while the peak position slightly shifts to a higher magnetic field with Sb substitution. The FWHM shows a slight increase to 56.0(5) and 54.0(5) Oe at $T = 4.3 \text{ K}$ for Ag- or Sb-substituted samples, respectively. The FWHM is also found to increase slightly with decreasing temperature for Ag- or Sb-substituted samples. These observed values are also close to the previously reported values ($\sim 50 \text{ Oe}$) at room temperature [29].

The temperature dependence of K is shown in Fig. 2, where K is determined by the peak position of the spectrum. Although the absolute values of K depend on the sample composition, their temperature dependencies exhibit qualitatively the same behavior: K slightly decreases with decreasing temperature, then levels off at low temperatures. The temper-

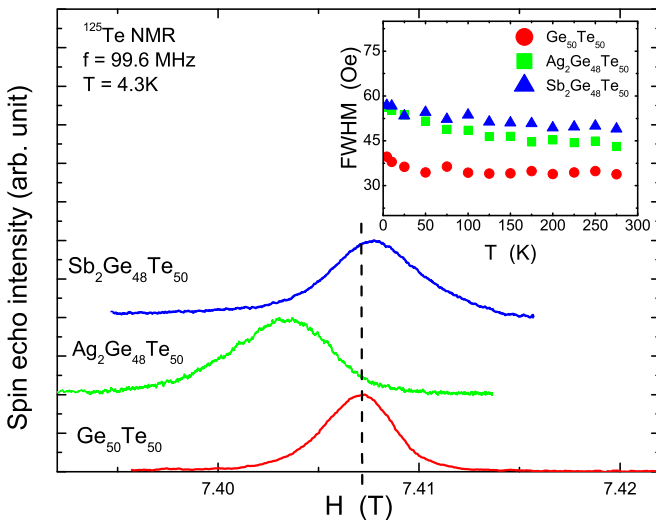


FIG. 1. Field-swept ^{125}Te -NMR spectra for $\text{Ge}_{50}\text{Te}_{50}$, $\text{Ag}_2\text{Ge}_{48}\text{Te}_{50}$, and $\text{Sb}_2\text{Ge}_{48}\text{Te}_{50}$ at $f = 99.6 \text{ MHz}$ and $T = 4.3 \text{ K}$. The dotted vertical line is a guide for the eyes. The inset shows the temperature dependence of FWHM for the samples.

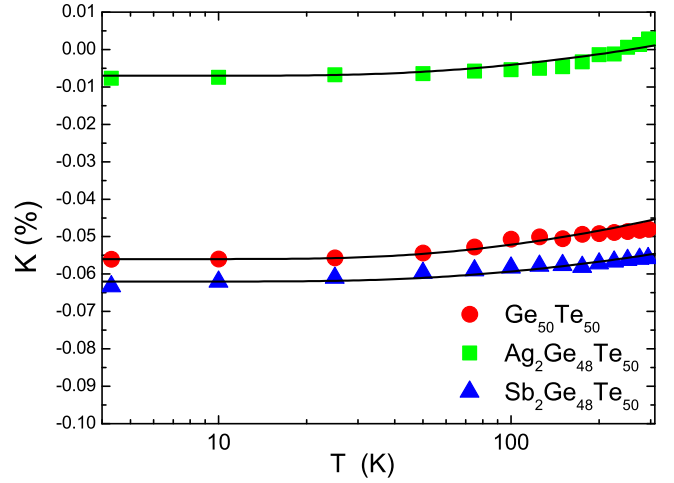


FIG. 2. Temperature dependence of NMR shift K for $\text{Ge}_{50}\text{Te}_{50}$ (red circles), $\text{Ag}_2\text{Ge}_{48}\text{Te}_{50}$ (green squares), and $\text{Sb}_2\text{Ge}_{48}\text{Te}_{50}$ (blue triangles). The solid lines are best fits using Eq. (2).

ature dependence of K can be analyzed by a two-band model, where the first band overlaps the Fermi level and the second band is separated from the Fermi level by an energy gap (E_g). The nearly temperature-independent behavior observed at low temperatures is a typical characteristic of metals (due to Pauli paramagnetic susceptibility) originating from the first band. The increase of K at high temperatures originates from the second band, similar to the case of semiconductors. Thus, the total NMR shift is given by

$$K = K_{\text{Pauli}} + K_{\text{semi}} + K_{\text{orb}}, \quad (1)$$

where K_{Pauli} is the temperature-independent NMR shift related to the Pauli paramagnetic susceptibility χ_{Pauli} due to self-doping/substitution effects and K_{semi} originates from the semiconductinglike nature giving rise to the temperature-dependent contribution because of thermal excitations across an energy gap E_g . The temperature-independent K_{orb} includes chemical shift, orbital, and Landau diamagnetic contributions. As is shown below, K_{orb} is estimated to be $-0.142(10)\%$. As the temperature-dependent K_{semi} has been calculated as $K_{\text{semi}} \propto \sqrt{T}e^{-E_g/k_B T}$ [30,31], the total K is given as

$$K = K_{\text{Pauli}} + a\sqrt{T}e^{-E_g/k_B T} + K_{\text{orb}}. \quad (2)$$

Using the $K_{\text{orb}} = -0.142(10)\%$ and $E_g/k_B = 67(4) \text{ K}$ [$5.8(3) \text{ meV}$] estimated from the temperature dependence of $1/T_1$ shown below, the experimental data are reasonably reproduced, as shown by the solid lines with $K_{\text{Pauli}} = 0.084\%$, $a = 0.00075\%/\sqrt{\text{K}}$ for $\text{Ge}_{50}\text{Te}_{50}$, $K_{\text{Pauli}} = 0.135\%$, $a = 0.00057\%/\sqrt{\text{K}}$ for $\text{Ag}_2\text{Ge}_{48}\text{Te}_{50}$, and $K_{\text{Pauli}} = 0.081\%$, $a = 0.00052\%/\sqrt{\text{K}}$ for $\text{Sb}_2\text{Ge}_{48}\text{Te}_{50}$, respectively. Since K_{Pauli} is proportional to the Pauli paramagnetic susceptibility, which is proportional to the density of states $\mathcal{N}(E_F)$ at the Fermi level, the increase of K_{Pauli} from $\text{Ge}_{50}\text{Te}_{50}$ to the Ag-doped material indicates an increase of $\mathcal{N}(E_F)$ while Sb doping reduces $\mathcal{N}(E_F)$ at the Fermi level. These results are consistent with the previous report [29]. The $\mathcal{N}(E_F)$ discussed here is due to unavoidable self-doping and/or Ag(Sb)-substitution effects,

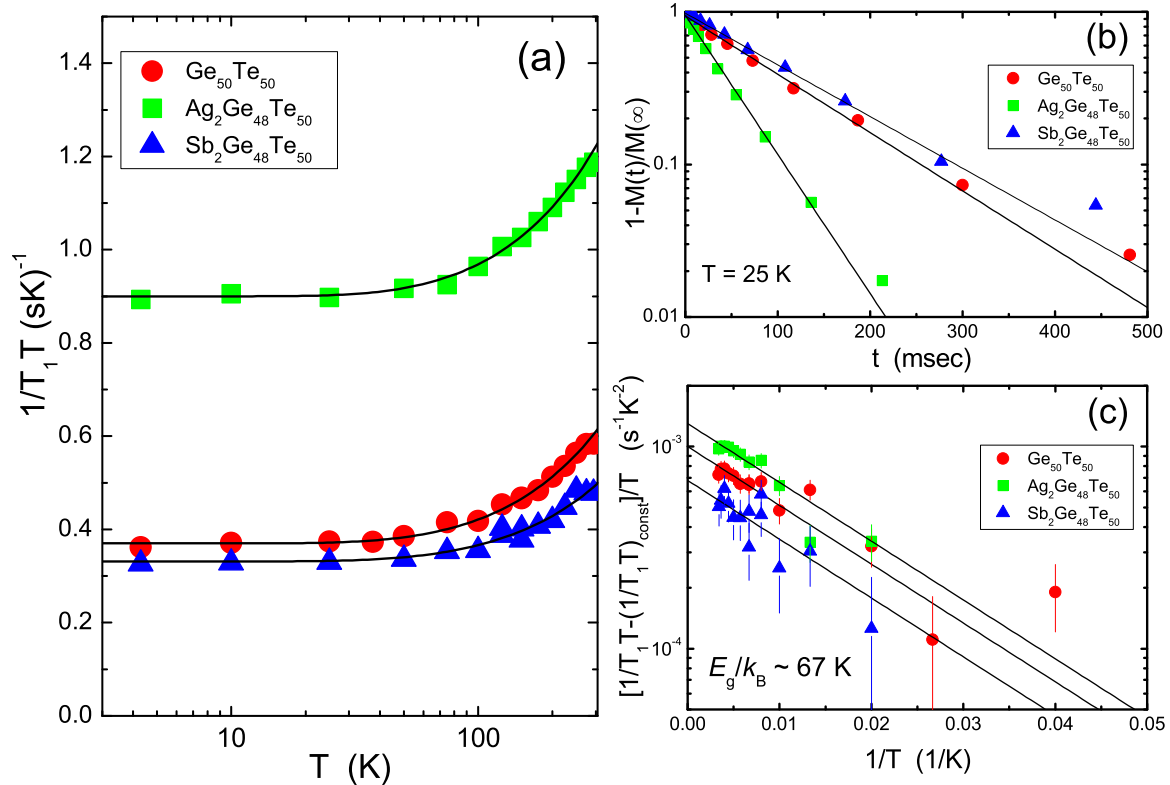


FIG. 3. (a) Temperature dependence of ^{125}Te $1/T_1T$ for $\text{Ge}_{50}\text{Te}_{50}$ (red circles), $\text{Ag}_2\text{Ge}_{48}\text{Te}_{50}$ (green squares), and $\text{Sb}_2\text{Ge}_{48}\text{Te}_{50}$ (blue triangles). The solid lines are best fits with the equation of $1/T_1T = (1/T_1T)_{\text{const}} + Ae^{-E_g/k_B T}$ for each sample. (b) Typical nuclear recovery curves for the three samples at $T = 25$ K. (c) Semilog plot of $[1/T_1T - (1/T_1T)_{\text{const}}]/T$ vs $1/T$. The solid lines are fitting results with $E_g/k_B = 67(4)$ K.

not including the effects of thermally activated carriers from the second band.

Figure 3(a) shows the temperature dependence of $1/T_1T$ for the three samples. T_1 values reported here were measured by the single saturation rf pulse method at the peak position of the NMR spectrum. As shown in Fig. 3(b), the nuclear recovery data can be fitted by a single exponential function $1 - M(t)/M(\infty) = e^{-t/T_1}$, where $M(t)$ and $M(\infty)$ are the nuclear magnetizations at time t after the saturation and the equilibrium nuclear magnetization at $t \rightarrow \infty$, respectively. Similar to the case of K , $1/T_1T$'s for all samples exhibit qualitatively the same behavior: $1/T_1T$ decreases slightly with decreasing temperature, then levels off at low temperatures. The temperature dependence of $1/T_1T$ can also be explained by the two-band model.

In this case, $1/T_1T$ is given by

$$1/T_1T = (1/T_1T)_{\text{const}} + Ae^{-E_g/k_B T}, \quad (3)$$

where $(1/T_1T)_{\text{const}}$ is the temperature-independent constant value originating from the conduction carriers and the second term is due to thermal excitation effects from the second band [31,32]. Here, we assumed in the simple model [Eq. (3)] that a cross-relaxation effect originated from mixing of the two bands is negligible, for simplicity. A similar analysis of the temperature dependence of $1/T_1T$ without the cross-relaxation process has been reported in the semimetal $\text{CaAl}_{2-x}\text{Si}_{2+x}$ [33] and in the Heusler-type compound $\text{Fe}_{2+x}\text{V}_{1-x}\text{Al}$ [34].

Using Eq. (3), the magnitude of E_g is estimated to be 67(4) K for $\text{Ge}_{50}\text{Te}_{50}$ and $\text{Ag}_2\text{Ge}_{48}\text{Te}_{50}$, although the experimental data are somewhat scattered, as shown in Fig. 3(c), where $[1/T_1T - (1/T_1T)_{\text{const}}]/T$ is plotted against $1/T$ on a semilog scale. It is difficult to estimate E_g for $\text{Sb}_2\text{Ge}_{48}\text{Te}_{50}$ due to a large scattering of the data. The black solid line in the figure is the best fit with an assumption of $E_g/k_B = 67$ K, which seems to reproduce the data reasonably well, although we cannot determine E_g . It is noted that 67 K is too small to attribute it to the semiconducting gap energy of 0.3–0.5 eV reported from optical measurements for GeTe [21].

The solid lines in Fig. 3(a) are best fits to Eq. (3), using $E_g/k_B = 67$ K, with $(1/T_1T)_{\text{const}} = 0.37$ (sK^{-1}), $A = 0.0013$ (sK^2) $^{-1}$ for $\text{Ge}_{50}\text{Te}_{50}$, $(1/T_1T)_{\text{const}} = 0.90$ (sK^{-1}), $A = 0.0010$ (sK^2) $^{-1}$ for $\text{Ag}_2\text{Ge}_{48}\text{Te}_{50}$, and $(1/T_1T)_{\text{const}} = 0.33$ (sK^{-1}), $A = 0.00068$ (sK^2) $^{-1}$ for $\text{Sb}_2\text{Ge}_{48}\text{Te}_{50}$, respectively. Within a Fermi liquid picture, $(1/T_1T)_{\text{const}}$ is proportional to the square of the density of states at the Fermi level $\mathcal{N}(E_F)$ and K_{Pauli} is proportional to $\mathcal{N}(E_F)$. Therefore, as K_{Pauli} is expected to be proportional to $(1/T_1T)_{\text{const}}^{1/2}$, one can estimate the temperature-independent K_{orb} by plotting $(1/T_1T)_{\text{const}}^{1/2}$ as a function of the temperature-independent $K = K_{\text{Pauli}} + K_{\text{orb}}$ at low temperatures for different samples. As shown in Fig. 4, we actually found a linear relation between $(1/T_1T)_{\text{const}}^{1/2}$ and K in the plot of $(1/T_1T)_{\text{const}}^{1/2}$ versus the temperature-independent K , from which K_{orb} is estimated to be $-0.142(10)\%$.

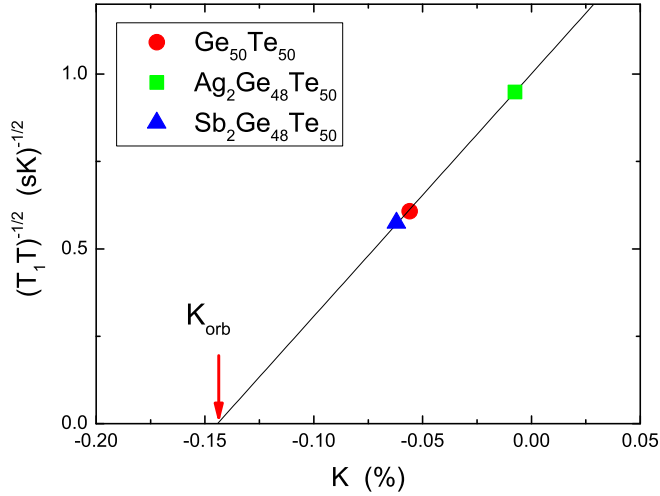


FIG. 4. $(1/T_1 T)_{\text{const}}^{0.5}$ vs the temperature-independent $K = K_{\text{Pauli}} + K_{\text{orb}}$ for the three samples. The solid line is a linear fit giving rise to $K_{\text{orb}} = -0.142(10)\%$.

Using the NMR data, we can discuss electron correlations through the Korringa ratio analysis. As described, both $(1/T_1 T)_{\text{const}}$ and K_{Pauli} are determined primarily by $\mathcal{N}(E_F)$. This leads to the general Korringa relation

$$T_1 T K_{\text{spin}}^2 = \frac{\hbar}{4\pi k_B} \left(\frac{\gamma_c}{\gamma_N} \right)^2 \equiv R, \quad (4)$$

where K_{spin} denotes the spin part of the NMR shift. For the ^{125}Te nucleus, $R = 2.637 \times 10^{-6}$ Ks. Deviations from R can reveal information about the electron correlations in materials, which are conveniently expressed via the Korringa ratio $\alpha \equiv R/(T_1 T K_{\text{spin}}^2)$ [35,36]. For uncorrelated metals, one has $\alpha \sim 1$. For antiferromagnetic spin correlations, $\alpha \gg 1$; in contrast, $\alpha \ll 1$ for ferromagnetic spin correlations. The Korringa ratio α , then, reveals how electrons correlate in materials. Figure 5 shows the temperature dependence of α for the three samples. We found the values of α for all samples are similar, $\alpha \sim 1.25$ at low temperatures, where the temperature-independent $(1/T_1 T)_{\text{const}}$ and K_{Pauli} dominate, indicative of no strong correlations for conduction carriers originating from self-doping/substitution effects in the samples. With increasing temperature, α slightly increases above ~ 50 K. If we assume that the Korringa relation holds at high temperatures, the increase suggests a tiny enhancement of antiferromagnetic spin correlations for carriers. Since the temperature dependence of α originates from the second band having a semiconducting nature, these results may suggest that thermally excited carriers play an important role in the electron correlation effects in the system.

As electron correlations have been pointed out to be significant for a figure of merit (zT values) [37], it is interesting if the increase of zT in $\text{Ge}_{50}\text{Te}_{50}$ at high temperatures above 300 K [7] is related to the electron correlations. Further NMR studies at high temperatures above 300 K are required to shed light on the relationship between the electron correlations and zT , which is currently in progress.

We now discuss how the carrier concentration changes by Ag or Sb substitution based on $\mathcal{N}(E_F)$ obtained from

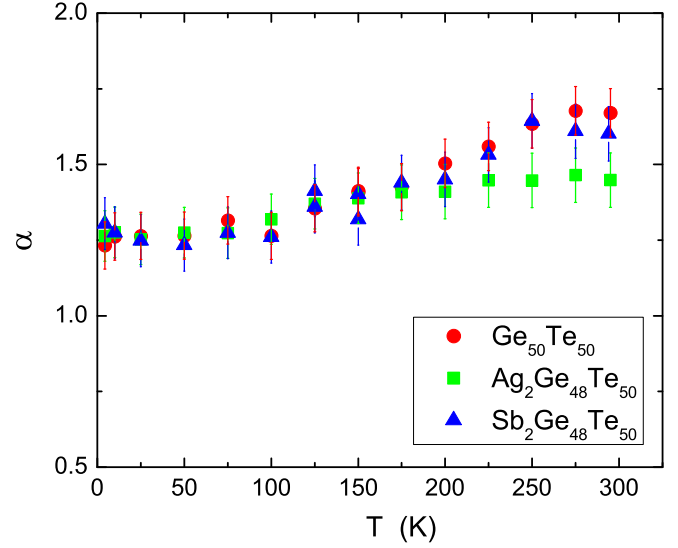


FIG. 5. Temperature dependence of the Korringa ratio α for $\text{Ge}_{50}\text{Te}_{50}$ (red circles), $\text{Ag}_2\text{Ge}_{48}\text{Te}_{50}$ (green squares), and $\text{Sb}_2\text{Ge}_{48}\text{Te}_{50}$ (blue triangles)

NMR data. In a parabolic band for noninteracting carriers, $\mathcal{N}(E_F)$ is given by $\mathcal{N}(E_F) = \frac{4\pi}{h^3} (2m^*)^{3/2} E_F^{1/2}$, where $E_F = \frac{\hbar^2}{2m^*} (3\pi^2 n)^{2/3}$. Here, n is the carrier concentration and m^* the renormalized effective carrier mass. Therefore, one can get a simple relation of $\mathcal{N}(E_F) \propto (m^* n^{1/3})$. From the values of $(1/T_1 T)_{\text{const}}$ and/or K_{Pauli} where the effect from m^* can be negligible, the carrier concentration in $\text{Ag}_2\text{Ge}_{48}\text{Te}_{50}$ is found to increase about 380% from that of $\text{Ge}_{50}\text{Te}_{50}$ while the carrier concentration in $\text{Sb}_2\text{Ge}_{48}\text{Te}_{50}$ is reduced only by $\sim 16\%$. Since there are $1.85 \times 10^{22} \text{ cm}^{-3}$ Ge atoms in $\text{Ge}_{50}\text{Te}_{50}$, the replacement of two Ag atoms for two Ge atoms out of 50 provides an additional $7.4 \times 10^{20} \text{ cm}^{-3}$ holes into the system. On the other hand, the substitution of two Sb atoms should reduce the same amount of carrier concentration ($7.4 \times 10^{20} \text{ cm}^{-3}$). Therefore, the large increase of the carrier concentration by Ag substitution and the slight decrease of that by Sb substitution cannot be explained by the simple substitution effect. These results strongly indicate that the number of Ge vacancies must be different for Ag or Sb substitutions. A similar conclusion has been pointed out in our previous paper [29].

To obtain insight into the origin of the metallic conductivity in $\text{Ge}_{50}\text{Te}_{50}$, particularly the vacancy effects on the electronic structure of $\text{Ge}_{50}\text{Te}_{50}$, we performed first-principles calculations where we employed a full-potential linear augmented plane wave method (FP-LAPW) [38] with a generalized gradient approximation (GGA) functional [39]. We constructed supercells which are composed of 27 Ge atoms and 27 Te atoms and randomly chose sites for the vacancies or for the Ag-substituted site. To obtain the self-consistent charge density, we employed $R_{\text{MT}} k_{\text{max}} = 7.0$ and $R_{\text{MT}} = 2.3$ and 2.8 a.u. for Ge and Te atoms, respectively. We selected 828 \mathbf{k} points in the irreducible Brillouin zone to obtain the self-consistent charge and density of states (DOS). As convergence criteria, we used an energy difference 0.0001 Ry/cell, charge difference 0.0001 e , and force difference 1.0 mRy/a.u. between

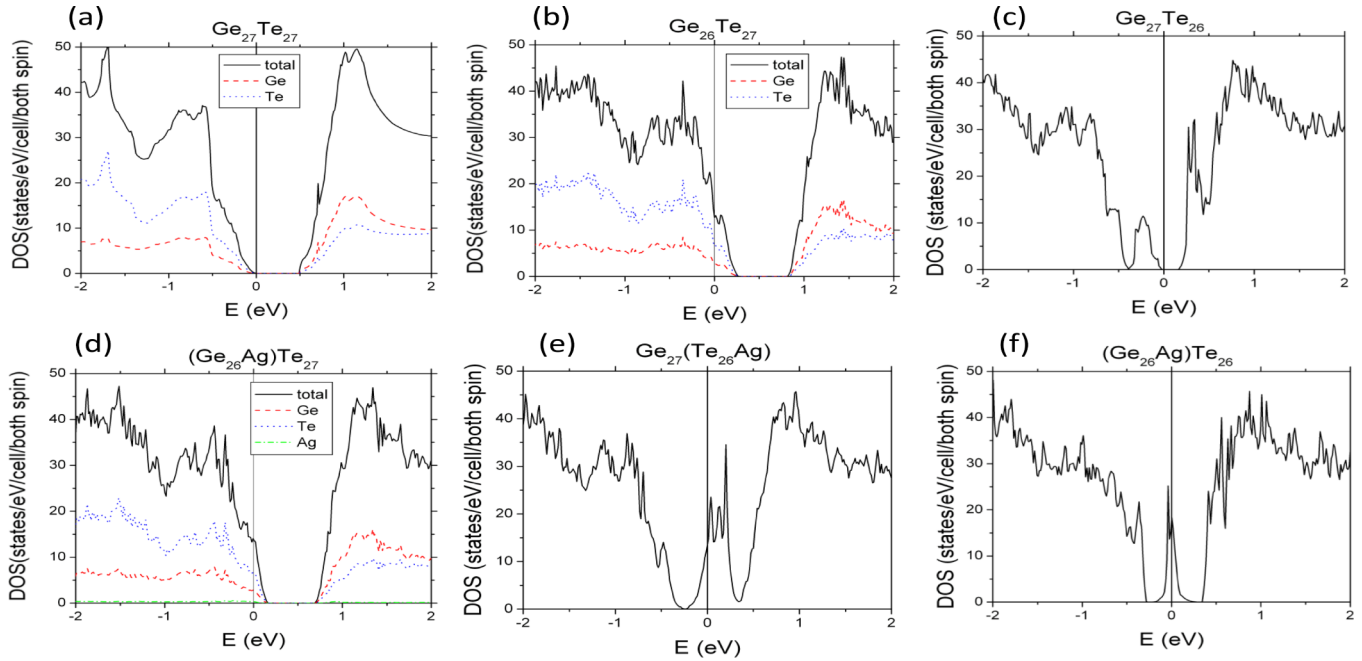


FIG. 6. Density of states (DOS) near the Fermi level (E_F). The black line is the total DOS. In some figures, atomic decomposed DOS is shown where the blue and red dotted lines show DOS from Te 5p and Ge 4p electrons, respectively: (a) $\text{Ge}_{27}\text{Te}_{27}$, (b) $\text{Ge}_{26}\text{Te}_{27}$, (c) $\text{Ge}_{27}\text{Te}_{26}$, (d) $(\text{Ge}_{26}\text{Ag})\text{Te}_{27}$, (e) $\text{Ge}_{27}(\text{Te}_{26}\text{Ag})$, and (f) $(\text{Ge}_{26}\text{Ag})\text{Te}_{26}$.

self-consistent steps. To get an optimized structure, we relaxed atoms around the vacancy or the substituted atom so that forces on each atom are less than 2.0 mRy/a.u.

Figure 6(a) shows the calculated DOS for a perfect $\text{Ge}_{27}\text{Te}_{27}$ without any defect, with a band gap of ~ 0.5 eV (semiconductor nature). This agrees well with previous reports [15,16,20]. Here, we show atomic decomposed DOS of the perfect $\text{Ge}_{27}\text{Te}_{27}$, where the black line shows the total DOS. The red and blue dotted lines show DOS from Te 5p and Ge 4p electrons, respectively. Figures 6(b) and 6(c) show the vacancy effect on DOS. In the case of a vacancy at the Ge site ($\text{Ge}_{26}\text{Te}_{27}$), the Fermi level E_F moves to a lower energy while keeping a similar gap structure to the case of $\text{Ge}_{27}\text{Te}_{27}$. This produces a finite DOS at E_F , giving rise to a metallic character. Most of the DOS at E_F originates from Te 5p and Ge 4p electrons. On the other hand, a vacancy at the Te site ($\text{Ge}_{27}\text{Te}_{26}$) keeps the semiconducting states, although some isolated states develop in the gap. We conclude that a vacancy at the Ge site gives rise to *p*-type metallic conductivity in $\text{Ge}_{50}\text{Te}_{50}$, as has been observed in experiments. A similar conclusion based on electronic structure calculations has been reported by Edwards *et al.* [20]. We further investigate the Ag-substitution effect on the electronic states. Figures 6(d) and 6(e) show an Ag-atom-substitution effect on DOS. While replacing a Ge atom by an Ag atom lowers the Fermi level and gives a metallic character, as in the case of a Ge vacancy, replacing a Te atom develops some isolated states in the gap and places E_F on the isolated states. Finally, Fig. 6(f) shows DOS for a case where an Ag atom replaces a Ge atom and a vacancy on the Te atom site. In this case the impurity states are sharper than other cases and E_F is located at the center of the isolated states. As we discussed, our NMR data were well explained by the two-band model, where one band overlaps the Fermi level,

giving a metallic nature, and the other band is separated from the Fermi level by an energy gap of $E_g/k_B = 67(4)$ K. It is clear that the metallic band can be attributed to the Ge vacancy effect, while the second band cannot be explained by the effect. We found that a vacancy at the Te sites produces an isolated state in the gap, and one may think that it could be the origin of the second band. However, our observation of a gap magnitude of 67(4) K [5.8(3) meV] is much smaller than the gap energy of order (0.1 eV), even if we take the isolated states created by the Te defects into consideration. Therefore, we consider that the observed semiconducting nature cannot be attributed to the Te-defect effects but probably fine structures of DOS near the Fermi level.

Finally, it is interesting to point out the inhomogeneity of the electronic states in the samples. According to Levin *et al.* [28], electronic inhomogeneity has been observed in some semiconductors, such as PbTe, from $1/T_1$ measurements. We investigate the homogeneity of electronic states in the samples by measuring T_1 at $T = 4.3$ K and different positions in the spectra for the three samples. As shown in Figs. 7(a)–7(c), $1/T_1$ seems to depend on the position in the spectrum, where we plotted $1/T_1 T$ together with the corresponding spectrum. Here, it is noted that, since our H_1 for T_1 measurement is ~ 25 Oe, which is much smaller than the linewidth of the observed spectrum, we cannot saturate the whole spectrum with the single rf pulse. What we have measured is an average value of T_1 for a part of the line saturated by the rf pulse. For each position, we observed a nearly single exponential behavior in nuclear recovery. This is probably due to a small distribution of T_1 in the saturated part of the line, although T_1 depends on its position in the spectrum, as shown in Figs. 7(a)–7(c). One can see that $1/T_1$ has a trend of a slight increase at lower magnetic field positions, indicating a greater

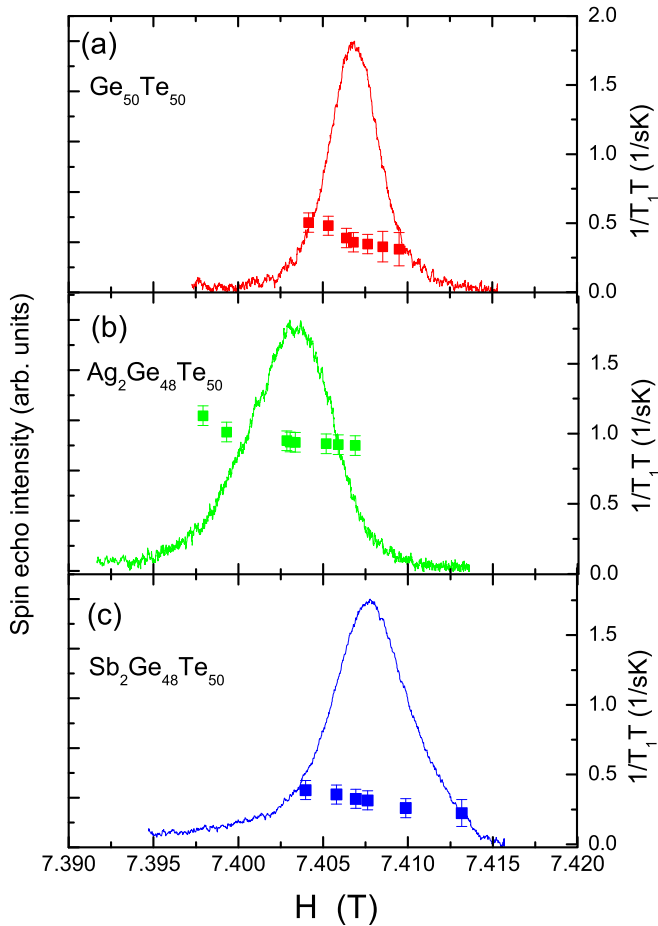


FIG. 7. Position dependence of $1/T_1T$ at $T = 4.3$ K for (a) $\text{Ge}_{50}\text{Te}_{50}$, (b) $\text{Ag}_2\text{Ge}_{48}\text{Te}_{50}$, and (c) $\text{Sb}_2\text{Ge}_{48}\text{Te}_{50}$, together with the corresponding NMR spectrum.

K_{spin} . For example, the $1/T_1T$ at the peak position of $\text{Ge}_{50}\text{Te}_{50}$ is ~ 0.36 (sK) $^{-1}$, while the $1/T_1T \sim 0.50$ (sK) $^{-1}$ at a lower field position ($H = 7.4033$ T). The enhancement of $1/T_1T$ and the larger K_{spin} at lower magnetic fields are consistent with an increased carrier concentration. Since $1/T_1T$ and K_{spin} values are related to $\mathcal{N}(E_F)$, this result indicates that the electronic state in $\text{Ge}_{50}\text{Te}_{50}$ is likely inhomogeneous. Similar behaviors have been observed in $\text{Ag}_2\text{Ge}_{48}\text{Te}_{50}$ and $\text{Sb}_2\text{Ge}_{48}\text{Te}_{50}$. These results indicate electronic states of all GeTe-based materials investigated here are inhomogeneous, which could originate from a possible inhomogeneous dis-

tribution of defects creating areas with differing carrier concentrations in $\text{Ge}_{50}\text{Te}_{50}$ and $M_2\text{Ge}_{48}\text{Te}_{50}$ ($M = \text{Ag}, \text{Sb}$). The distributions of the local carrier concentration $\Delta n/n$ at low temperatures can be estimated from the distribution of the NMR shift, $\Delta K/K_{\text{spin}}$, where ΔK was estimated from the FWHM of the NMR spectrum at $T = 4.3$ K. From the relation of $\Delta n/n = (\Delta K/K_{\text{spin}})^3$, $\Delta n/n$ are estimated to be 0.25, 0.17, and 0.67 for $\text{Ge}_{50}\text{Te}_{50}$, $\text{Ag}_2\text{Ge}_{48}\text{Te}_{50}$, and $\text{Sb}_2\text{Ge}_{48}\text{Te}_{50}$, respectively. Using the average local carrier concentration $n = 8.0 \times 10^{20} \text{ cm}^{-3}$ ($\text{Ge}_{50}\text{Te}_{50}$), $1.7 \times 10^{20} \text{ cm}^{-3}$ ($\text{Ag}_2\text{Ge}_{48}\text{Te}_{50}$), and $4.0 \times 10^{20} \text{ cm}^{-3}$ ($\text{Sb}_2\text{Ge}_{48}\text{Te}_{50}$) obtained from the Hall coefficient measurement [29], Δn are estimated to be $2.0 \times 10^{20} \text{ cm}^{-3}$, $2.9 \times 10^{20} \text{ cm}^{-3}$, and $2.7 \times 10^{20} \text{ cm}^{-3}$, respectively.

IV. CONCLUSION

We have carried out ^{125}Te NMR measurements to microscopically investigate the electronic properties of $\text{Ge}_{50}\text{Te}_{50}$, $\text{Ag}_2\text{Ge}_{48}\text{Te}_{50}$, and $\text{Sb}_2\text{Ge}_{48}\text{Te}_{50}$. For $\text{Ge}_{50}\text{Te}_{50}$, the NMR shift K and $1/T_1T$ data are nearly temperature independent at low temperatures below ~ 50 K and both increase slightly with increasing temperature at high temperatures. These behaviors are well explained by a two-band model, where one band overlaps the Fermi level and the other band is separated from the Fermi level by an energy gap of $E_g/k_B = 67(4)$ K. A Korringa analysis indicates that the conduction carriers can be considered as free carriers with no significant electron correlations at low temperatures. On the other hand, the Korringa ratio increases slightly at high temperatures, suggesting a slight enhancement of the electron correlation. A first-principles calculation revealed that the metallic band originates from the Ge vacancy while the semiconductorlike band may be related to the fine structure of the density of states near the Fermi level. Low-temperature ^{125}Te NMR data for $\text{Ag}_2\text{Ge}_{48}\text{Te}_{50}$ and $\text{Sb}_2\text{Ge}_{48}\text{Te}_{50}$ clearly demonstrate that the carrier concentration changes by Ag or Sb substitutions, where the Ag substitution increases hole concentration while Sb substitution decreases the concentration.

ACKNOWLEDGMENTS

The research was supported by the U.S. Department of Energy, Office of Basic Energy Sciences, Division of Materials Sciences and Engineering. Ames Laboratory is operated for the U.S. Department of Energy by Iowa State University under Contract No. DE-AC02-07CH11358.

- [1] R. A. Hein, J. W. Gibson, R. Mazelsky, R. C. Millerand, and J. K. Hulm, *Phys. Rev. Lett.* **12**, 320 (1964).
- [2] E. F. Steigmeier and G. Harbeke, *Solid State Commun.* **8**, 1275 (1970).
- [3] J. Akola and R. O. Jones, *Phys. Rev. Lett.* **100**, 205502 (2008).
- [4] G. J. Snyder and E. S. Toberer, *Nat. Mater.* **7**, 105 (2008).
- [5] J. P. Heremans, V. Jovovic, E. S. Toberer, A. Saramat, K. Kurosaki, A. Charoenphakdee, S. Yamanaka, and G. J. Snyder, *Science* **321**, 554 (2008).
- [6] E. A. Skrabek and D. S. Trimmer, *CRC Handbook of Thermoelectrics* (CRC Press, Boca Raton, FL, 1995).
- [7] E. M. Levin, M. F. Besser, and R. Hanus, *J. Appl. Phys.* **114**, 083713 (2013).
- [8] D. Wu, L.-D. Zhao, S. Hao, Q. Jiang, F. Zheng, J. W. Doak, H. Wu, H. Chi, Y. Gelbstein, C. Uher, C. Wolverton, M. Kanatzidis, and J. He, *J. Am. Chem. Soc.* **136**, 11412 (2014).
- [9] R. Sankar, D. P. Wong, C.-S. Chi, W.-L. Chien, J.-S. Hwang, F.-C. Chou, L.-C. Chen, and K.-H. Chen, *CrystEngComm* **17**, 3440 (2015).
- [10] S. K. Plachkova, *Phys. Status Solidi A* **83**, 349 (1984).
- [11] B. A. Cook, M. J. Kramer, X. Wei, J. L. Harringa, and E. M. Levin, *J. Appl. Phys.* **101**, 053715 (2007).

- [12] E. M. Levin, S. L. Bud'ko, and K. Schmidt-Rohr, *Adv. Funct. Mater.* **22**, 2766 (2012).
- [13] F. Herman, R. L. Kortum, I. B. Ortenburger, and J. P. Van Dyke, *J. Phys. Colloq.* **29**, C4-62 (1968).
- [14] M. L. Cohen, Y. Tung, and P. B. Allen, *J. Phys. Colloq.* **29**, C4-163 (1968).
- [15] H. M. Polatoglou, G. Theodorou, and N. A. Economou, in *Physics of Narrow Gap Semiconductors* (Springer, Berlin, 1982), pp. 221–225.
- [16] D. J. Singh, *J. Appl. Phys.* **113**, 203101 (2013).
- [17] D. H. Damon, M. S. Lubeli, and R. M. Mazelsky, *J. Phys. Chem. Solids* **28**, 520 (1967).
- [18] N. V. Kolomoets, E. Y. Lev, and L. M. Sysoeva, *Sov. Phys. Semicond.* **5**, 2101 (1964).
- [19] N. V. Kolomoets, E. Y. Lev, and L. M. Sysoeva, *Sov. Phys. Solid State* **6**, 551 (1964).
- [20] A. H. Edwards, A. C. Pineda, P. A. Schultz, M. G. Martin, A. P. Thompson, H. P. Hjalmarsen, and C. J. Umrigar, *Phys. Rev. B* **73**, 045210 (2006).
- [21] P. M. Nikolic, *J. Phys. D* **2**, 383 (1969).
- [22] M. S. Lubell and R. Mazelsky, *J. Electrochem. Soc.* **110**, 520 (1963).
- [23] Y. Gelbstein, O. Ben-Yehuda, E. Pinhas, T. Edrei, Y. Sadia, Z. Dashevsky, and M. P. Dariel, *J. Electron. Mater.* **38**, 1478 (2009).
- [24] Y. Gelbstein, B. Daro, O. Ben-Yehuda, Y. Sadia, Z. Dashevsky, and M. P. Dariel, *J. Electron. Mater.* **39**, 2049 (2010).
- [25] L. Zhang, W. Wang, B. Ren, and Y. Yan, *J. Electron. Mater.* **40**, 1057 (2011).
- [26] R. Wolfe, J. H. Wernick, and S. E. Haszko, *J. Appl. Phys.* **31**, 1959 (1960).
- [27] J. P. Heremans and C. M. Jaworski, *Appl. Phys. Lett.* **93**, 122107 (2008).
- [28] E. M. Levin, J. P. Heremans, M. G. Kanatzidis, and K. Schmidt-Rohr, *Phys. Rev. B* **88**, 115211 (2013).
- [29] E. M. Levin, *Phys. Rev. B* **93**, 045209 (2016).
- [30] D. Wolf, *Spin Temperature and Nuclear Spin Relaxation in Matter* (Clarendon, Oxford, UK, 1979).
- [31] N. Bloembergen, *Physica* **20**, 1130 (1954).
- [32] G. Al, G. Frosali, and O. Morandi, in *Scientific Computing in Electrical Engineering*, edited by A. M. Anile, G. Alì, and G. Mascali, Mathematics in Industry Vol. 9 (Springer, Berlin, 2004), p. 271.
- [33] C. S. Lue, S. Y. Wang, and C. P. Fang, *Phys. Rev. B* **75**, 235111 (2007).
- [34] C. S. Lue and Joseph H. Ross, Jr., *Phys. Rev. B* **61**, 9863 (2000).
- [35] T. Moriya, *J. Phys. Soc. Jpn.* **18**, 516 (1963).
- [36] A. Narath and H. T. Weaver, *Phys. Rev.* **175**, 373 (1968).
- [37] A. V. Joura, D. O. Demchenko, and J. K. Freericks, *Phys. Rev. B* **69**, 165105 (2004).
- [38] P. Blaha, K. Schwarz, G. K. H. Madsen, D. Kvasnick, and J. Luitz, *WIEN2K, an Augmented Plane Wave + Local Orbitals Program for Calculation Crystal Properties* (Karlheinz Schwarz, Technical Universität Wien, Austria, 2001).
- [39] J. P. Perdew, K. Burke, and M. Ernzerhof, *Phys. Rev. Lett.* **77**, 3865 (1996).